Synthesis, structural characterisation and thermoelectric properties of Bi1−xPbxOCuSe

Article

Accepted Version

Journal Name

Dynamic Article Links ►

Cite this: DOI: 10.1039/c0xx00000x

www.rsc.org/xxxxxx

ARTICLE TYPE

Synthesis, structural characterisation and thermoelectric properties of $Bi_{1-x}Pb_xOCuSe$

Son D. N. Luu[a] and Paz Vaqueiro*[a]

Received (in XXX, XXX) Xth XXXXXXXXX 20XX, Accepted Xth XXXXXXXXX 20XX

DOI: 10.1039/b000000x

The effect of Pb^{2+} doping on the structure and thermoelectric properties of BiOCuSe (also known as BiCuSeO or BiCuOSe) is described. With increasing Pb^{2+} content, the expansion of the unit cell results in a weakening of the bonding between the $[Bi_{2(1-x)}Pb_{2x}O_2]^{2(1-x)+}$ and the $[Cu_2Se_2]^{2(1-x)-}$ layers. The electrical resistivity and Seebeck coefficient decrease in a systematic way with growing Pb^{2+} levels. The thermal conductivity rises due to the increase of the electronic contribution with doping. The power factor of materials with a 4-5% Pb^{2+} content takes values of *ca.* 8 μW cm^{-1} K^{-2} over a wide temperature range. ZT at 673 K is enhanced by *ca.* 50% when compared to values found for other dopants, such as Sr^{2+} or Mg^{2+}.

Introduction

Thermoelectric devices can convert waste heat directly into electricity, and offer the promise of a more efficient use of existing energy resources. The efficiency of thermoelectric power generation is largely determined by the performance of the thermoelectric materials that constitute the device. This efficiency is given by a figure of merit, ZT, related to the Seebeck coefficient (S), electrical conductivity (σ) and thermal conductivity (κ) of the material by $ZT = S^2\sigma T/\kappa$.[1] The need for thermoelectric devices with higher efficiencies has led to a tremendous growth of research into new thermoelectric materials.[2]

Lowering the thermal conductivity of a material without significantly reducing the power factor ($S^2\sigma$) would result in an increased figure of merit. For this reason, recent research strategies for the design of new thermoelectric materials have focused on reducing the thermal conductivity. For instance, in the "phonon glass electron crystal" approach, materials contain oversized cages in which "rattling" atoms produce a phonon damping effect which results in a reduced thermal conductivity.[3] Nanostructuring of thermoelectric materials can lead to reduced thermal conductivity through increased phonon scattering at the interfaces.[4] "Natural superlattice" materials, in which layers with excellent electronic transport properties are combined with a second type of layer which serves as a phonon scatterer, can also exhibit low thermal conductivities.[5] Examples of "natural superlattice" materials include layered cobalt oxides, such as $Ca_3Co_4O_9$ and $NaCo_2O_4$, which have a remarkable thermoelectric performance at elevated temperatures,[6] or the misfit layered compounds $(SnS)_{1+x}(TiS_2)$, with a ZT of 0.37 at 773 K.5 More recently, it has been reported that oxychalcogenides BiOCuQ (Q = Se, Te) have promising thermoelectric properties. For instance, BiOCuSe exhibits a ZT of 0.76 at 873 K, upon partial substitution of Bi^{3+} with Sr^{2+},[7] whilst BiOCuTe has a ZT of 0.66 at the maximum temperature investigated, 673 K.[8]

The BiOCuQ (Q = S, Se, Te) phases are members of a family of oxychalcogenides with the general formula AOBQ (A = La, Ce, Nd, Pr, Bi; B = Cu, Ag and Q = S, Se, Te).[9] These materials crystallise in the ZrSiCuAs structure, which consists of alternating $[A_2O_2]^{2+}$ and $[B_2Q_2]^{2-}$ layers stacked along the *c*-axis (Figure 1).

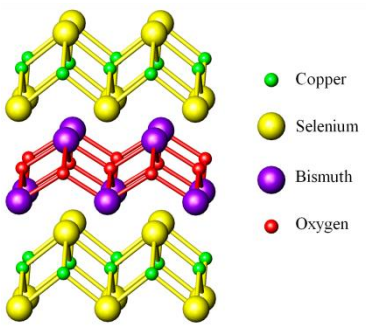

Figure 1. View of the crystal structure of BiOCuSe along the [010] direction.

The AOBQ phases, which are isostructural to the superconducting oxypnictides LnOFePn (Ln = La, Pr, Ce, Sm; Pn = P and As), have been primarily investigated for their optoelectronic properties, as many of them are transparent p-type semiconductors.[10] However, whilst the rare-earth oxychalcogenides are wide-band semiconductors, it has been found that the BiOCuQ phases have smaller band gaps, due to the contribution of the Bi 6*p* orbitals to the conduction band minima.9[(e)] Their lower band gap and higher electrical conductivities may make these materials attractive for thermoelectric applications. Although the lowest band gap is

found for the oxytelluride, efforts to date have focused on the selenium-containing phase. Ohtani *et al.* showed that BiOCuSe can be successfully doped by aliovalent substitution at the bismuth site or through copper deficiency.[11] Doped $Bi_{1-x}Sr_xOCuSe$ and $BiOCu_{1-x}Se$ were found to exhibit significantly reduced electrical resistivities (with a metal-like temperature dependence) when compared to BiOCuSe.[11] Subsequent studies of the thermoelectric properties found that $Bi_{1-x}Sr_xOCuSe$ and $BiOCu_{1-x}Se$ exhibit reasonable values of the power factor at elevated temperatures, combined with a low thermal conductivity.[7,12] It has been also shown that ball milling of BiOCuSe[13] or $Bi_{1-x}Ba_xOCuSe$ to reduce grain sizes leads to improvements in performance, with ZT reaching 1.1 at 923 K for $Bi_{0.875}Ba_{0.125}OCuSe$.[14] Here, a detailed account of the structural, electrical and thermal transport properties of $Bi_{1-x}Pb_xOCuSe$ samples prepared by solid state reactions followed by hot pressing, is presented.

Experimental

Synthesis

Samples of polycrystalline $Bi_{1-x}Pb_xOCuSe$ ($0 \leq x \leq 0.2$) were prepared by solid-state reaction between Bi_2O_3 (99.99%, Sigma Aldrich), Bi (99.5%, Aldrich), PbO_2 (99.5%, BHD Chemicals), Cu (99.5%, Johnson Matthey) and elementary Se (99.99%, Aldrich) using evacuated and sealed silica tubes ($< 10^{-4}$ Torr). Each stoichiometric mixture was first heated up to 623 K for 20 h and then up to 773 K for 10 h with a 2 K min^{-1} ramp rate. A second annealing process at 873 K for a further 7 h was carried out after regrinding the obtained powders. For electrical and thermal property measurements, the as-prepared powders were hot-pressed into highly densified pellets (≥ 95% of theoretical density) at 853 K and a uniaxial pressure of 50 bars for 30 minutes under a N_2 flow.

Structural and microstructural characterisation

Samples were characterised by powder X-ray diffraction using a Bruker D8 Advance Powder X-ray diffractometer, operating with germanium monochromated $CuK_{\alpha 1}$ radiation (λ = 1.54046 Å) and fitted with a LynxEye detector. Data were collected over a range of $5 \leq 2\theta/^o \leq 120$ for a period of 7 hours. Rietveld refinements were carried out using the GSAS software.[15] A FEI Quanta 650 FEG ESEM was used to study the morphology of pristine and doped samples.

Thermogravimetric analysis

A DuPont 951 thermogravimetric analyzer was employed to investigate the thermal stability of BiOCuSe at elevated temperatures. The sample was loaded into a platinum crucible and heated from room temperature to 973 K with a rate of 2 K min^{-1} under a N_2 or an O_2 flow.

Electrical transport measurements

The electrical resistivity of the sample over the temperature range $100 \leq T/K \leq 300$ was measured using a 4-probe DC technique. For each sample, a rectangular bar (~$6 \times 3 \times 1$ mm^3) was cut from a hot-pressed pellet. Four 50 μm silver wires were attached using silver paint and connections were made to a Keithley 2182 nanovoltmeter and a TTi QL564P power supply. The sample was mounted in an Oxford Instruments CF1200 cryostat connected to an ITC502 temperature controller. To measure the Seebeck coefficient over the same temperature range, the sample bar (~$6 \times 3 \times 1$ mm^3) was mounted on a copper holder, which incorporates a small heater (120 Ω strain gauge) located close to one end of the sample. The copper holder is attached to the hot stage of a closed-cycle refrigerator (DE-202, Advanced Research Systems), which is connected to a Lakeshore LS-331 temperature controller. Two 50 μm copper wires were attached to the ends of the sample bar using silver paint and connections made to a Keithley 2182A nanovoltmeter. Two Au: 0.07% Fe vs. chromel thermocouples were placed at the hot and cold ends of the sample, and connected to a second Lakeshore LS-331 temperature controller. The Seebeck coefficient at a given temperature was determined by applying a temperature gradient, ΔT, across the sample and measuring the corresponding thermal voltage, ΔV. The slope of the line, ΔV/ΔT, was used to determine the Seebeck coefficient.

For measurements above room temperature ($300 < T/K < 673$), the resistivity and Seebeck coefficient of each sample were measured simultaneously using Linseis LSR-3 instrument (Germany). Resistivity and Seebeck coefficient measurements were carried perpendicular to the pressing direction of the ingots, and in selected samples, parallel to the pressing direction.

Thermal transport measurements

An Anter FL3000 system was employed for measuring thermal diffusivity (α) and the heat capacity (C_p) of samples over a temperature range of $373 \leq T/K \leq 673$ in 50 K steps. Samples were hot-pressed into highly densified pellets with an approximate diameter of 13 mm and a thickness of 1-2 mm. A graphite coating on surface of pellet was applied to maximize heat absorption. The pellet was then loaded into the sample chamber which was purged with N_2 during the measurement. The thermal conductivity (κ) was calculated from the relationship $\kappa = \alpha C_p \rho$ where ρ is the sample density. A reference material, PyroceramTM 9606, of known heat capacity was used as a reference for the determination of the heat capacity of sample. The details of procedure of determination of the heat capacity are described in Ref. 16. Thermal conductivity measurements were carried out parallel to the pressing direction of the ingots.

Results and discussion

Structural and microstructural characterisation

Powder X-ray diffraction data collected on as-prepared samples of $Bi_{1-x}Pb_xOCuSe$ with compositions over the range $0 \leq x \leq 0.20$ indicate that these materials crystallise in the ZrSiCuAs structure (Figure 1). Most samples are single phases, with the exception of $x = 0.15$ for which a trace amount of Bi_2O_3 can be detected. In sharp contrast with a previous report which suggested that the maximum doping level was $x = 0.07$,[17] we have found that lead can be incorporated up to a doping level of $x \approx 0.20$. This is comparable to the solubility limit found for other divalent cations, such as Sr^{2+} and Ba^{2+}, for which doping contents of $x = 0.15$ have been reported.[7,14] Values of x greater than 0.2 result in samples containing significant amounts of impurities. The lower doping level reported in Ref. 17 might be related to the use of elemental lead for the synthesis of these phases, given that as-purchased

elemental lead often contains some lead oxide.

Rietveld refinements using powder X-ray diffraction data were carried out for the as-prepared samples of $Bi_{1-x}Pb_xOCuSe$ ($0 \leq x \leq 0.20$). A representative example of final observed, calculated and difference profiles for the X-ray diffraction data is shown in Figure 2, while remaining Rietveld profiles, tables of refined parameters, selected distances and angles have been included as Supplementary Information.

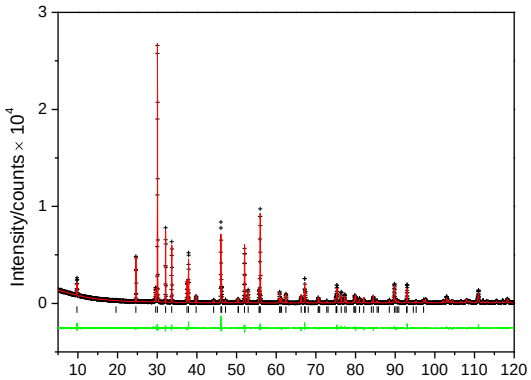

Figure 2. Rietveld refinement using powder X-ray diffraction data for $Bi_{0.825}Pb_{0.175}OCuSe$ (R_{wp} = 11.5%).

The lattice parameters of $Bi_{1-x}Pb_xOCuSe$ increase with increasing x (Figure 3 (a)). This increase, which is more noticeable along the *c*-axis, may be related to the larger ionic radius of Pb^{2+} (129 pm) when compared to that of Bi^{3+} (117 pm).[18] The expansion of the unit cell along the *c* axis leads to an increase of the Bi-Se distances (Figure 3(b)), which may indicate a weakening of the bonding between the oxide and chalcogenide layers with increasing lead content. The α and β Se-Cu-Se angles (Figure 3(c)) also change with increasing lead content, and this results in a reduction of the distortion of the $CuSe_4$ tetrahedra. As discussed previously for the isostructural oxytelluride,8 the thermal parameter of the copper site is significantly larger than those of the other three crystallographic sites, and this may be related to copper deficiency in the $[Cu_2Se_2]^{2-}$ layers.

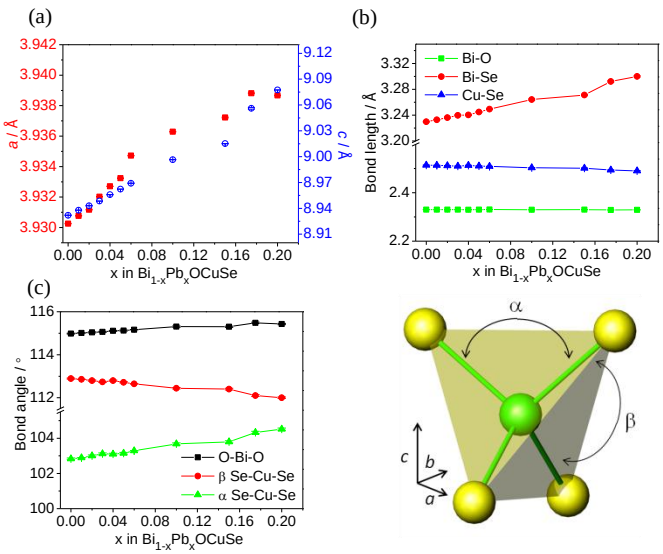

Figure 3. (a) Lattice parameters, (b) selected bond distances, and (c) selected bond angles in $Bi_{1-x}Pb_xOCuSe$. The $CuSe_4$ polyhedron is shown on the right.

Powder X-ray diffraction data collected on hot-pressed samples indicates that the ZrSiCuAs structure is retained, and no decomposition of the samples is observed (Supplementary Information). Diffraction measurements on hot-pressed ingots show no evidence of preferred orientation, and therefore the thermoelectric properties of samples prepared by hot pressing can be assumed to be isotropic. However, hot pressing leads to a marked broadening of all of the diffraction peaks, which may be indicative of microstrain. Examination of selected as-prepared and hot-pressed samples by electron microscopy (Figure 4) indicates that the as-prepared samples contain plate-like grains, with a thickness of *ca.* 0.2 μm and lengths of ~ 2 μm. The grains observed on fractured surfaces of hot-pressed ingots have similar plate-like shapes, although grain growth has clearly occurred.

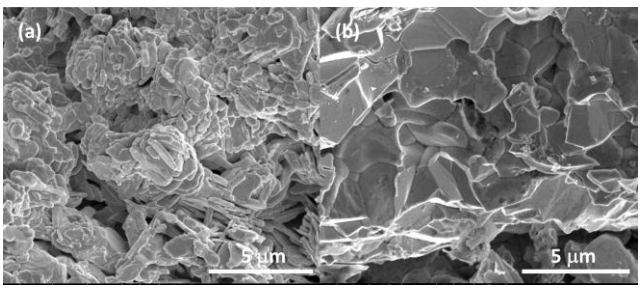

Figure 4. SEM micrographs for (a) as-synthesised BiOCuSe; (b) hot-pressed $Bi_{0.8}Pb_{0.2}OCuSe$.

Thermal stability

Thermogravimetric analysis, collected under a N_2 atmosphere indicates that BiOCuSe is stable up to the maximum temperature investigated, 973 K. However, when measurements are carried out in an O_2 atmosphere, the sample weight starts to increase at *ca.* 653 K, indicating that oxidation is occurring (Figure 5). Taking this into account, we have limited our study of the thermoelectric properties of these materials to the temperature range $100 \leq T/K \leq 673$, although incorporation of these materials in thermoelectric devices for operation at higher temperatures would be feasible under a protective atmosphere. This is the approach already adopted for PbTe-containing thermoelectric devices.[19]

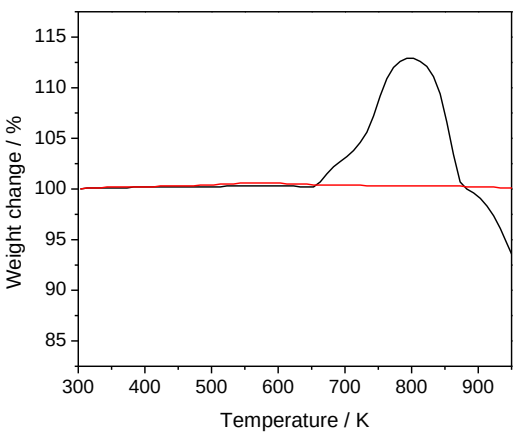

Figure 5. Thermogravimetric data for BiOCuSe collected under a N_2 (red line) and an O_2 atmosphere (black line).

Electrical and thermal transport properties

The electrical resistivity of undoped BiOCuSe is rather low over the whole temperature range (Figure 6). In contrast to a previous report on BiOCuSe prepared by cold pressing and sintering,9[e] which shows semiconducting behaviour, the electrical resistivity of our undoped BiOCuSe over the temperature range $100 \leq T/K \leq 550$ increases with increasing temperature, a temperature dependence which is consistent with degenerate semiconducting behaviour. The difference between the cold-pressed and the hot-pressed materials may be related to the lower density of the former, which will lead to a significant contribution of grain boundaries to the overall sample resistance. For samples prepared by spark plasma sintering (SPS), metal-like behaviour is observed at low temperatures, although at temperatures above 400 K the temperature dependence becomes characteristic of semiconducting behaviour.7 A maximum in the resistivity is also found for our hot-pressed BiOCuSe, but in this case the maximum occurs at approximately 550 K. It is well known that hot pressing or SPS can cause changes in stoichiometry (e.g. oxygen deficiency) or reduction, as the graphite in the die often acts as a reducing agent at high temperatures.[20] Although powder X-ray diffraction data collected on hot-pressed samples indicate that they have the same purity as the starting powders, small changes in stoichiometry caused by the pressing process cannot be excluded, and this could account for the difference between hot-pressed and SPS samples. Measurements on ingots cut perpendicular and parallel to the pressing direction show no significant changes in the Seebeck coefficient or electrical resistivity. This is consistent with the lack of preferred orientation observed in our X-ray diffraction measurements.

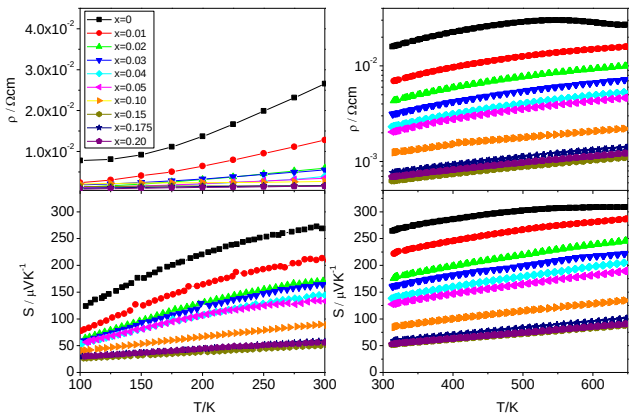

Figure 6. Electrical resistivity and Seebeck coefficient for $Bi_{1-x}Pb_xOCuSe$ as a function of temperature. High-temperature resistivity data are shown on a logarithmic scale for clarity.

The Seebeck coefficient of the undoped sample is positive, indicating that the electrical transport properties are dominated by holes, and is consistent with p-type semiconducting behaviour. For this family of oxychalcogenides, p-type conduction is normally observed,[9] and is attributed to the formation of a covalent hybridised band between Cu and Se atoms at the top of the valence band.[10] However, the origin of this p-type behaviour may also be related to copper deficiency, which can generate mobile holes.

The electrical resistivity of the doped samples decreases in a systematic way with increasing level of doping, and this is consistent with a rise in charge carrier concentration. Pb^{2+} is a very effective dopant, as shown by the large enhancement of the electrical conductivity at relatively low levels of doping: at room temperature the electrical conductivity increases from 63 S cm^{-1} for BiOCuSe to ~ 500 S cm^{-1} for $Bi_{0.95}Pb_{0.05}OCuSe$. By comparison, doping with 5% of Ba^{2+} results in a conductivity of 250 S cm^{-1},[14] and with 5% of Sr^{2+} in only 100 S cm^{-1}.7 The Seebeck coefficient, which remains positive, also decreases with increasing doping levels.

Whilst there is excellent agreement between the low- and high-temperature values of the Seebeck coefficient for each sample, the low-temperature resistivity data is affected by greater uncertainties in sample dimensions, as well as by the Peltier effect arising from the use of a constant dc current source.3[b] For this reason, low-temperature resistivity data have not been used in a quantitative way, and the power factor (Figure 7) has been calculated only for the temperature range $300 < T/K < 673$. For samples with $x \leq 0.05$, the power factor decreases slightly with increasing temperature, whilst for higher doping levels, the power factor shows a marked increase with increasing temperature. The highest values of the power factor have been found for samples with a Pb^{2+} content between 4 and 10%, at the maximum temperature investigated. Our hot-pressed materials exhibit higher power factors than those prepared by SPS.[17] Given that the processing conditions of thermoelectric materials can have a significant effect on their final performance, further optimisation of the consolidation process may lead to additional improvements in thermoelectric performance.

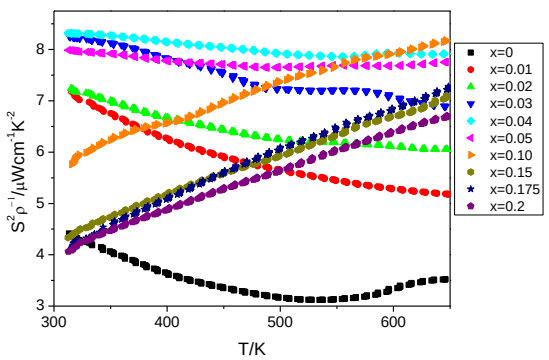

Figure 7. Power factor for $Bi_{1-x}Pb_xOCuSe$ as a function of temperature.

Although the power factors of these materials are moderate in comparison to that of Bi_2Te_3 (~ 40 μW cm^{-1} K^{-2}),[21] their magnitude is similar to those of other thermoelectric materials such as Zn_4Sb_3 (~ 13 μW cm^{-1} K^{-2} at 673 K).[22] Calculations of the band structure of BiOCuQ (Q = S, Se, Te) indicate that the top of the valence band consist of a mixture of light- and heavy-mass bands.[23] This has been shown to be a desirable feature for good thermoelectric performance,[24] as a light-mass band promotes good electrical conduction, whilst a heavy-mass band can lead to high Seebeck coefficients. However, the hole mobility in BiOCuSe, which is 20 cm^2 V^{-1} K^{-1}, is rather small, and decreases markedly with doping due to point-defect scattering.[25] As the

thermoelectric figure of merit is proportional to the mobility, according to the expression $Z \propto (m^*)^{3/2}\mu$ (where m^* is the effective mass and μ the mobility),[26] this can explain the moderate power factors observed for these materials.

The thermal conductivity as a function of temperature for the $Bi_{1-x}Pb_xOCuSe$ series is shown in Figure 8. The total thermal conductivity we found for BiOCuSe (0.97 W m^{-1} K^{-1} at 373 K) is comparable to previously reported values,7 and significantly lower than that of Bi_2Te_3 (~ 2 W m^{-1} K^{-1}).[21] The electronic and lattice contributions were estimated using the electrical conductivity data in conjunction with the Wiedemann-Franz law, with a Lorenz constant of 2.45×10^{-8} W Ω K^{-2}. For BiOCuSe, the electronic contribution is only *ca.* 4% of the total thermal conductivity. The total thermal conductivity rises with increasing lead content up to 1.58 W m^{-1} K^{-1} at 373 K for $Bi_{0.8}Pb_{0.2}OCuSe$. The electronic thermal conductivity for doped samples increases markedly with x. This indicates that the rise in the total thermal conductivity with doping originates from the increase in electronic thermal conductivity caused by growing charge carrier concentrations. It has been suggested that the remarkably low thermal conductivity of BiOCuSe arises from the two-dimensional nature of the structure of this material, which leads to scattering of phonons at the interfaces between the $[Cu_2Se_2]^{2-}$ and $[Bi_2O_2]^{2+}$ layers.7,[13] This is supported by the low sound speed and a low Young's modulus of BiOCuSe, which may be indicative of weak bonding between layers.[13] Moreover, band structure calculations on these phases indicate that the bonding is highly anisotropic,[27] and that the nature of the bonding between the oxide and chalcogenide layers is mainly ionic and weaker than the intralayer bonding.9[(e)]

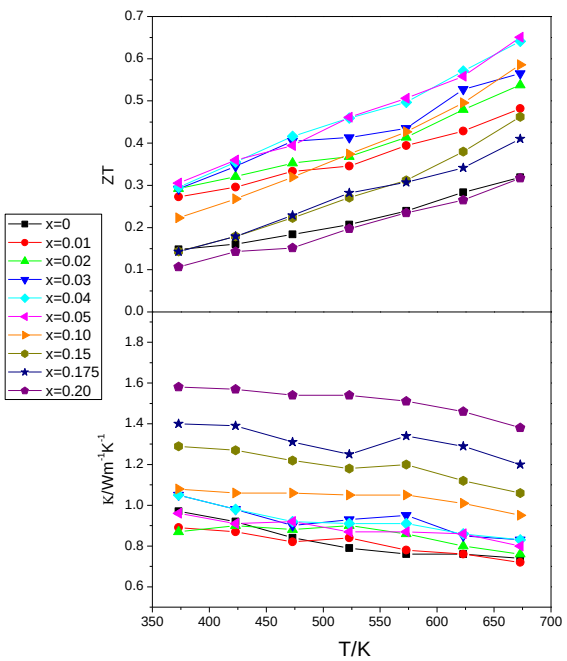

Figure 8. Thermal conductivity and figure of merit for $Bi_{1-x}Pb_xOCuSe$ as a function of temperature.

The thermoelectric figure of merit as a function of temperature is shown in Figure 8. For all compositions investigated, ZT increases with increasing temperature up to the maximum temperature investigated. Given the trend shown by these data, we would expect that even higher values of ZT would be achieved at higher temperatures. However, as shown by our thermogravimetric data (Figure 5), use of these materials at higher temperatures would require the use of a protective atmosphere to prevent oxidation. The values found for the undoped material are comparable to those previously reported by Zhao *et al.*7 The maximum value of ZT, which is 0.65 at 673 K, is found for doping levels of 4-5% lead. This represents an improvement of *ca.* 50% when compared with values found for other dopants at the same temperature. For example, at 673 K, a ZT ≈ 0.35 is found for x = 0.15 in $Bi_{1-x}Sr_xOCuSe$,[7] ZT reaches *ca.* 0.3 for x = 0.985 in $BiOCu_{1-x}Se$,[12] and a ZT ≈ 0.3 has been determined for x = 0.125 in $Bi_{1-x}Mg_xOCuSe$.[28] The performance of the materials reported here is comparable to that of ball-milled $Bi_{1-x}Ba_xOCuSe$, for which reduction of grain sizes to 200-400 nm decreases the thermal conductivity by *ca.* 40%, resulting in an improved ZT ≈ 0.6 at 673K for x = 0.10.[14] The enhanced performance of Pb-doped samples may be related to their slightly higher hole mobility when compared to those doped with Ba^{2+} or Sr^{2+},[17] as evidenced by the significantly higher electrical conductivities found for the same levels of doping. This may be related to the similarity in atomic masses of Pb^{2+} and Bi^{3+}, which may lessen point-defect scattering. Furthermore, for the materials described here, the distortion of the $CuSe_4$ tetrahedra (Figure 3(c)), which could be detrimental to the Cu 3*d* - Se 4*p* orbital mixing and hence to the hole mobility,[25] decreases with increasing levels of doping. This may also be a contributory factor to the higher hole mobility of the Pb-doped samples when compared to those containing other dopants.

Conclusions

We have demonstrated that Pb^{2+} doping in BiOCuSe results in a marked enhancement of the thermoelectric performance when compared to other dopants. Further improvements in the performance of these materials may be achieved by ball milling, given that it has been shown that the thermal conductivity of BiOCuSe can be reduced to 0.54 W m^{-1} K^{-1} at 300 K[14] through this process. This could result in materials with ZT > 1 at relatively low temperatures, which would be well suited for thermoelectric waste heat recovery.

Acknowledgements

We thank the Energy Technology Partnership and European Thermodynamics Ltd. for financial support for this project. Dr J.W.G. Bos is thanked for access to electrical transport measurement equipment.

Notes and references

[a] *Institute of Chemical Sciences, Heriot-Watt University, Edinburgh EH14 4AS, UK; E-mail: P.Vaqueiro-Rodriguez@hw.ac.uk*

† Electronic Supplementary Information (ESI) available: Rietveld profiles, tables of refined parameters, selected distances and angles; powder X-ray diffraction data of selected hot-pressed samples. See DOI: 10.1039/b000000x/

1 D.M. Rowe, Thermoelectrics Handbook: Macro to Nano, Ed. D.M. Rowe, CRC Press, Boca Raton, FL, 2006, Chapter 1.
2 J. R. Sootsman, D. Y. Chung, M. G. Kanatzidis, *Angew. Chem. Int. Ed*., 2009, **48**, 8616.
3 (a) G.A. Slack, CRC Handbook of Thermoelectrics, Ed. D.M. Rowe, Press, Boca Raton, FL, 1995, p. 407; (b) G.S. Nolas, J. Sharp, H.J. Goldsmid, Thermoelectrics: Basic Principles and New Materials Developments, Springer, Berlin Heidelberg, 2001.
4 P. Vaqueiro, A. V. Powell, *J. Mater. Chem.*, 2010, **20**, 9577.
5 C. Wan, Y. Wang, N. Wang, W. Norimatsu, M. Kusunoki, K. Koumoto, *Sci. Technol. Adv. Mater*., 2010, **11**, 044306.
6 I. Terasaki, Y. Sasago, K. Uchinokura, *Phys. Rev. B* 1997, **56**, R12685.
7 L.D. Zhao, D. Berardan, Y.L. Pei, C. Byl, L. Pinsard-Gaudart, N. Dragoe, *Appl. Phys. Lett.*, 2010, **97**, 092118.
8 P. Vaqueiro, G Guélou, M. Stec, E. Guilmeau, and A.V. Powell, J. Mater. Chem. A, 2013, **1**, 520.
9 (a) M. Palazzi, C. Carcaly, J. Flahaut, *J. Solid State Chem.* 1980, **35**, 150; (b) A.M. Kusainova, P.S. Berdonosov, L.G. Akselrud, L.N. Kholodkovskaya, V.A. Dolgikh, B.A. Popovkin, *J. Solid State Chem.* 1994, **112**, 189; (c) G.H. Chan, B.Den, M.Bertoni, J.R. Ireland, M.C. Hersam, T.O. Mason, R.P. Van Duyne, J.A. Ibers, *Inorg. Chem.* 2006, **45**, 8264; (d) M.L. Liu, L.B. Wu, F.Q. Huang, L.D. Chen, J.A. Ibers, *J. Solid State Chem.* 2007, **180**, 62; (e) H. Hiramatsu, H. Yanagi, T. Kamiya, K. Ueda, M. Hirano, H. Hosono, *Chem. Mater.* 2008, **20**, 326.
10 K. Ueda, H. Hiramatsu, M. Hirano, T. Kamiya, H. Hosono, *Thin Solid Films*, 2006, **496**, 8.
11 T. Ohtani, Y. Tachibana, Y. Fujii, *J. Alloys Comp.*, 1997, **262**, 175.
12 Y. Liu, L.-D. Zhao, Y. Liu, J. Lan, W. Xu, F. Li, B.-P. Zhang, D. Berardan, N. Dragoe, Y.-H. Lin, C.-W. Nan, J.-F. Li, H. Zhu, *J. Am. Chem. Soc.*, 2011, **133**, 20112.
13 F. Li, J.-F. Li, L.-D. Zhao, K. Xiang, Y. Liu, B.P. Zhang, Y.-H. Lin, C.-W. Nan, H.-M. Zhu, *Energy Environ. Sci.*, 2012, **5**, 7188.
14 J. Li, J. Sui, Y. Pei, C. Barreteau, D. Berardan, N. Dragoe, W. Cai, J. He, L.-D. Zhao, *Energy Environ. Sci.*, 2012, **5**, 8543.
15 A.C. Larson, R.B. von Dreele, General Structure Analysis System, Los Alamos Laboratory, 1994 [Report LAUR 85-748].
16 P.S. Gaal, S.P. Apostolescu, US Patent No. US 6,375,349, 2002.
17 L. Pan, D. Berardan, L. Zhao, C. Barreteau, N. Dragoe, *Appl. Phys. Lett.*, 2013, **102**, 023902.
18 R.D. Shannon, *Acta Cryst.*, 1976, A**32**, 751.
19 R.D. Abelson, Thermoelectrics Handbook: Macro to Nano, Ed. D.M. Rowe, CRC Press, Boca Raton, FL, 2006, Chapter 56.
20 R.W. Rice, Ceramic Fabrication Technology, Marcel Dekker, New York Basel, 2003.
21 H. Scherrer, S. Scherrer, CRC Handbook of Thermoelectrics, Ed. D.M. Rowe, CRC Press, Boca Raton, FL, 1995, Chapter 19.
22 T. Caillat, J.-P. Fleurial, A. Borshchevsky, *J. Phys. Chem. Solids* 1997, **58**, 1119.
23 D. Zou, S. Xie, Y. Liu, J. Lin, J. Li, *J. Mater. Chem. A*, 2013, **1**, 8888.
24 D.J. Singh, I.I. Mazin, *Phys. Rev. B*, 1997, **56**, R1650.
25 C. Barreteau, D. Bérardan, E. Amzallag, L.D. Zhao, N. Dragoe, *Chem. Mater.*, 2012, **24**, 3168.
26 C. Wood, *Rep. Prog. Phys.*, 1988, **51**, 459.
27 V. V. Bannikov, I. R. Shein, A.L. Ivanovskii, *Solid State Sci.*, 2012, **14**, 89.
28 J. Li, J. Sui, C. Barreteau, D. Berardan, N. Dragoe, W. Cai, Y. Pei, *J. Alloys Comp.*, 2013, **551**, 649.

